Mikhail N. Slipchenko
Weldon School of Biomedical Engineering,
Purdue University,
West Lafayette, IN 47907;
Spectral Energies, LLC,
Dayton, OH 45431

Clint E. Moody

Joseph D. Miller

Department of Mechanical Engineering,
Iowa State University,
Ames, IA 50011

Sukesh Roy
Spectral Energies, LLC,
Dayton, OH 45431

James R. Gord
Air Force Research Laboratory,
Wright-Patterson Air Force Base,
OH 45433

Terrence R. Meyer[1]
Department of Mechanical Engineering,
Iowa State University,
Ames, IA 50011
e-mail: trm@iastate.edu

Micro-Optical Initiation of Nanoenergetic Materials Using a Temporally Tailored Variable-Pulse-Width Laser

Nanoenergetic materials can provide a significant enhancement in the rate of energy release as compared with microscale materials. The energy-release rate is strongly dependent not only on the primary particle size but also on the level of agglomeration, which is of particular interest for the inclusion of nanoenergetics in practical systems where agglomeration is desired or difficult to avoid. Unlike studies of nanoparticles or nanometer-size aggregates, which can be conducted with ultrafast or nanosecond lasers assuming uniform heating, microscale aggregates of nanoparticles are more sensitive to the thermophysical time scale of the heating process. To allow control over the rate of energy deposition during laser initiation studies, a custom, temporally tailored, continuously variable-pulse-width (VPW) laser was employed for radiative heating of nanoenergetic materials. The laser consisted of a continuous-wave master oscillator, which could be sliced into desired pulses, and a chain of amplifiers to reach high peak power. The slicer allowed control over the time profile of the pulses via the combination of an arbitrary waveform generator and acousto-optic modulator (AOM). The effects of utilizing flat-top or ramped laser pulses with durations from 100 ns to 150 μs and energies up to 20 mJ at 1064 nm were investigated, along with a broad range of heating rates for single particles or nanoparticle aggregates up to 100-μm diameter. In combination with an optical microscope, laser heating of aggregates consisting of 70-nm diameter Al nanoparticles in a Teflon matrix showed significant dependence on the heating profile due to the sensitivity of nanoenergetic materials to heating rate. The ability to control the temporal pulse-intensity profile leads to greater control over the effects of ablative heating and the resulting shockwave propagation. Hence, flexible laser-pulse profiles allow the investigation of energetic properties for a wide size range of metal/metal-oxide nanoparticles, aggregates, and composites. [DOI: 10.1115/1.4007887]

Keywords: laser initiation, nanoenergetic materials, variable-pulse-width laser

1 Introduction

Nanoenergetic materials are currently being investigated for use as additives in propellant, explosive, and liquid-fuel formulations, as well as for use in nanomanufacturing [1–3]. Metal and metal-oxide particles with dimensions in the nanometer-size range provide a significant enhancement in the rate of energy release, although the physical mechanisms behind this enhancement are not fully understood. While the maximum energy density of a given energetic mixture can be deduced based on elemental properties and bulk thermochemistry, the release rate of this energy is strongly dependent on a wide range of conditions. These include the size and diameter of the metal nanoparticles, the thickness of the oxide shell or passivation layer, the loading ratio of the nanoparticles within a mixture or composite, and the nature of the oxidant species. An additional parameter that is often overlooked is the level of agglomeration, which is of particular interest for the inclusion of nanoenergetics in practical systems.

Laser-induced photothermal initiation has been exploited for the quantitative determination of properties such as ignition time and burn rate [4–6]. However, studies that measure reaction progress in bulk phase cannot predict the effects of size because of the large number of simultaneously sampled particles with a broad distribution of parameters [7,8]. To address these difficulties, spectroscopic studies of laser-initiated monodisperse nanoparticle reactions have been carried out [7,9–16]. In these studies, laser ignition of energetic materials was performed with weakly focused laser beams leading to simultaneous excitation of multiple isolated nanoparticles. It is difficult, however, to prepare samples of monodisperse aggregates of nanoparticles. In addition, because of the surface nature of laser heating [6], the thermal-diffusion length limits the aggregate particle size that can be uniformly heated with fixed temporal pulse width. For a laser pulse with a temporal width that is much shorter than the thermal-diffusion length scale, the fast rise in surface temperature will lead to ablation and shockwave propagation rather than uniform bulk heating. For illustration, Fig. 1(*a*) shows the thermal-diffusion length dependence on heating-pulse duration calculated using the thermal-diffusion coefficient for bulk aluminum (Al). Note that picosecond (ps) and nanosecond (ns) lasers are only suitable for submicrometer sized particles (left shaded area in Fig. 1(*a*)). However, aggregates can reach tens of micrometers in size (right shaded area in Fig. 1(*a*)). Therefore, a laser system with a pulse width in the range of tens of ns to tens of microseconds (μs) is needed for uniform laser initiation of nanoparticle aggregates. In addition, the absorbed laser energy required for starting the

[1]Corresponding author.

Manuscript received April 17, 2012; final manuscript received September 11, 2012; published online January 18, 2013. Assoc. Editor: Debjyoti Banerjee.

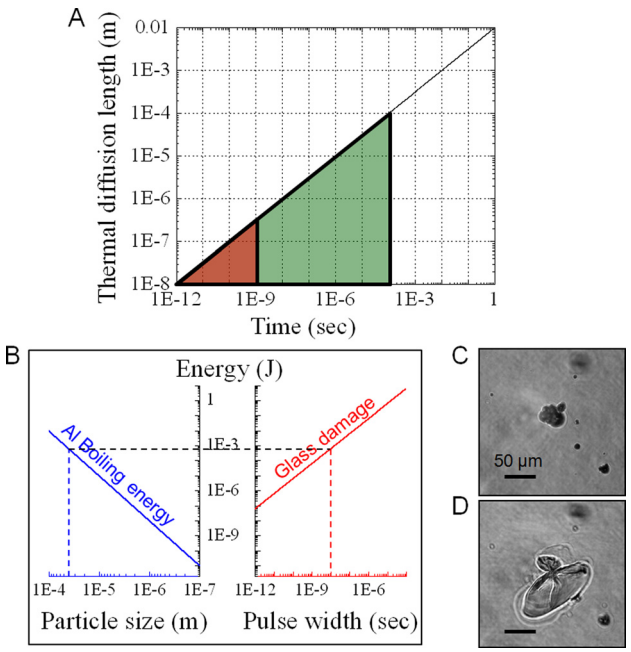

Fig. 1 Optimal laser-pulse duration and energy dependence on particle size. (*a*) Thermal-diffusion length for uniform heating of solid Al with given pulse time duration. Shaded areas roughly correspond to nanoparticles or aggregates of sizes less than 300 nm (left) and greater than 300 nm (right). (*b*) Illustration of how laser heating of large particle with fixed duration (10-ns) laser can be limited by damage threshold of dielectric substrate. (*c*) Optical image of 30-μm size Al aggregate placed on the surface of the cover slip. (*d*) Glass substrate damage as a result of initiation of aggregate in (*c*) by 1-mJ, 10-ns pulse.

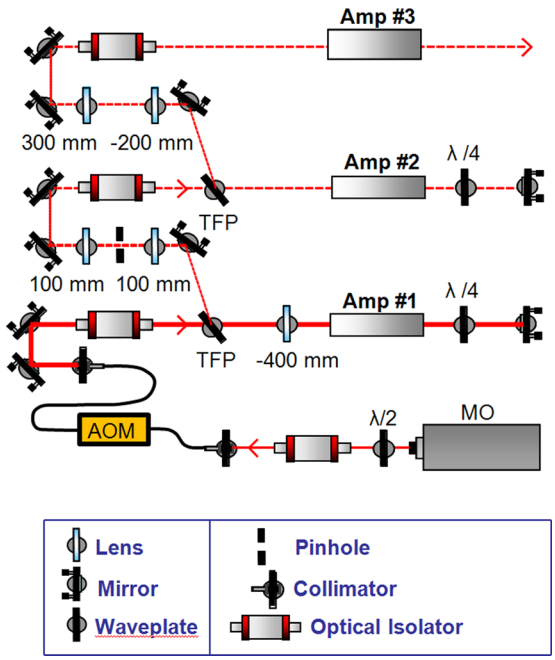

Fig. 2 Temporally tailored, variable-pulse-width laser layout: MO—master oscillator, AOM—fiber-pigtailed acousto-optic modulator, TPF—thin-film polarizer. Amp #1, Amp #2, and Amp #3 are Nd:YAG flashlamp amplifiers with 101-mm rod length and 4-mm, 5-mm, and 6.3-mm rod diameters, respectively.

reaction is proportional to particle mass and, therefore, scales as the cube of the particle size. Although short-pulse duration lasers have enough energy per pulse to evaporate mm-size particles, the damage threshold of dielectric materials used as substrates can limit the maximum energy. Since the peak power damage threshold for dielectric materials such as glass is a constant at tight focusing conditions [17], longer pulse durations are necessary for delivering the desired energy for large particles without exceeding the damage threshold. For example, as shown in Fig. 1(*b*), to heat a 40-μm Al particle to boiling temperature, the laser pulse width should be longer than 10 ns to avoid substrate damage. Figures 1(*c*)–1(*d*) shows the example of glass substrate damage as a result of large-aggregate flash heating by a 1-mJ, 10-ns pulse.

The continuous tuning of laser-pulse duration for varying the heating rate is straightforward from 100 femtosecond (fs) to 1 ns by pulse stretching of fs Ti:sapphire regenerative amplifiers [18], but tunability in the ns to μs regime is harder to achieve. One approach is to use a variable oscillator length via insertion of fibers of different length [19,20]. Such a system is capable of pulse-duration tuning from tens of ns to a few μs, but the pulse-width tuning requires replacement of the fiber. Here, we describe a simple and flexible method for flash heating of single nanoenergetic particles using temporal pulse shaping (variable temporal profile) and multistage amplification (variable output power), and we illustrate the importance of controlling the heating rate of nanoparticle aggregates. This is achieved through the development and application of a VPW Nd:YAG laser with continuously tunable pulse duration from 100 ns to 150 μs and with a temporally tailored pulse shape. The benefits of pulse shaping for controlling multiscale thermophysical processes is demonstrated for initiation of micron-scale aggregates of 70-nm diameter Al nanoparticles imbedded in a layer of Teflon, which acts as an oxidizer [9,12]. We observed two regimes of initiation that occur as a function of the temporal profile of the laser pulse, which we tentatively attribute to the presence or lack of initial ablation following the onset of laser heating.

2 Experimental Setup

2.1 Temporally Tailored, Variable-Pulse-Width Laser. The VPW laser incorporates a master oscillator power amplifier (MOPA) design as shown in Fig. 2. The master oscillator is a continuous wave (cw), Nd:YAG diode-pumped laser at 1064 nm (I4-300mW-SLM-1064, Elforlight) with an average power of ~300 mW. The cw light is shaped with a programmable AOM to control the duration and temporal profile of the pulse. A fiber-pigtailed AOM module (T-M200-0.1C2G-3-F2P, Gooch and Housego, Florida) is used to obtain an extinction ratio of 10^6 between pulse peak power and broad temporal background to avoid heating of particles outside the laser-pulse duration. The VPW output of the AOM is amplified by two double-pass amplification stages and one single-pass stage. Each stage is pumped by a flashlamp with a duration of up to 1.5 ms. The amplified pulse is delayed by 400 μs with respect to the flashlamp, corresponding to the maximum gain of each amplifier stage, thus producing a relatively flat temporal pulse profile. The energy of the output pulse is controlled by the flashlamp pulse energy of each amplifier. For initiation of nanoenergetic materials, the laser is operated in a single-pulse mode, although it can also be operated in a burst mode [21]. The pulse width can be varied from 15 ns to 1 ms, limited by both the temporal resolution of the AOM and the nearly uniform gain region of the flashlamp-pumped amplifiers. For the present experiment, full-width-half-maximum (FWHM) pulse widths in the range of 100 ns to 50 μs were used. This includes a slowly ramped pulse with a full duration of 150 μs. The typical pulse energy at 1064 nm is ~20 mJ for a 10-μs laser pulse, corresponding to ~2 kW peak power. Further details of laser amplification levels and temporal control of laser pulses are described in Sec. 3.

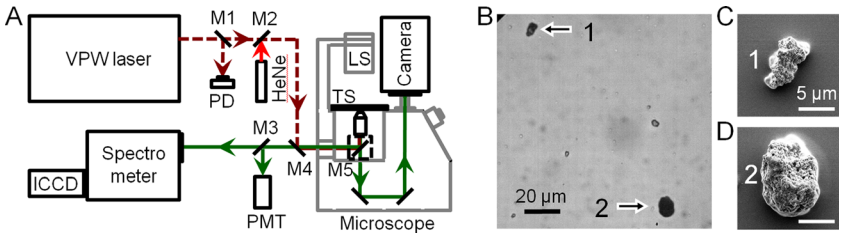

Fig. 3 Experimental setup for micro-optical initiation and optical and SEM images of aggregates. (*a*) Coupling of VPW laser to micro-optical test bench. PD—photodiode, HeNe—632-nm helium–neon laser, LS—light source with a condenser, TS—motorized XY translational stage, PMT—photomultiplier tube, M1—10% beam splitter, M2—632-nm dielectric mirror, M3—10% beam splitter, M4—1064-nm dielectric mirror, M5—50% beam splitter or silver mirror. (*b*) Optical images of aggregates. (*c*) and (*d*) SEM images of individual aggregates indicated in (*b*).

2.2 Micro-Optical Imaging and Microspectroscopy. A schematic of the micro-optical imaging and spectroscopy system is shown in Fig. 3(*a*). A portion (10%) of the energy from the 1064-nm output of the VPW laser is sent to a photodiode (DET10A, Thorlabs) for recording the temporal profile of the laser pulses. For alignment purposes, the 632-nm output of the HeNe laser is combined with the 1064-nm beam using a 632-nm dielectric mirror. The 1064-nm beam and a portion of 632-nm beam are directed into an inverted microscope (Axiovert 10, Zeiss) using a 1064-nm dielectric mirror (M4 in Fig. 3(*a*)), and both are focused into the sample with a 100× air objective (NA = 0.95). The resulting focus spot is estimated based on micro-optical images to be about 1 μm, which is smaller than the particle-aggregate dimensions.

To precisely control and record the target sample position, the microscope is equipped with a large-area XY motorized translation stage (Max202, Thorlabs) with 40-nm minimal step size and 1-μm repeatability. Signal from the sample is collected utilizing the same objective. A beam splitter installed under the objective sends 80% of the signal toward an ultrahigh frame-rate CMOS camera (SA5, Photron) for resolving the time-dependence of emission from initiated nanoenergetic particles. A 750-nm short-pass filter is installed in the camera beam path to block stray scattering of the 1064-nm laser pulse. The remaining 20% of the emission is sent to a 303-mm focal length ultraviolet–visible (UV–vis) spectrometer (Shamrock SR-303i-A, Andor Technologies) equipped with a gated intensified CCD camera (PI-Max ICCD, Princeton Instruments). Prior to the signal reaching the spectrometer, another beam splitter sends 10% of that signal to a photomultiplier tube (PMT, 931B, Hamamatsu) for recording the time trace of the spectrally integrated emission signal from either 330 to 550 nm or 500 to 640 nm.

2.3 Sample Preparation and Characterization. Teflon-coated Al particles were prepared in a manner similar to that described by Yang et al. [12,22]. Here, microscale agglomerates consisting of approximately 70-nm primary particles (Alfa Aesar, product #45546) were spin-coated with Teflon oxidizer onto a cover slip of 170-μm thickness. The primary particle size of 70 nm was verified to within ±10% using a scanning electron microscope (SEM, Quanta 250 FEG, FEI). No precaution was taken to remove the oxide layer, with a thickness estimated to be in the 2.5-nm to 3-nm range [23]. To immobilize the particle and to confine the ablated material within the oxidizer matrix, a second layer of Teflon ~100-μm thick was applied to enclose large aggregates within the oxidizer matrix. Optical images of typical agglomerates are shown in Fig. 3(*b*). Their agglomerated nature is clearly visible in the SEM images shown in Figs. 3(*c*) and 3(*d*), which were taken prior to application of the second 100-μm thick Teflon coating. The reported results are representative data from a total of 35 laser initiation experiments.

3 Results and Discussion

3.1 VPW Laser Performance. Distortion-free amplification of the AOM-shaped output of the cw Nd:YAG seed laser requires that the gain in the amplifying medium is not depleted by the pulse itself. Hence, the flashlamp amplifiers should be operated in the small-signal gain regime for which the extracted energy does not change the gain of the amplifiers, particularly that of the last in the chain because it is delivering the highest energy. Assuming a maximum acceptable gain depletion of 10%, we can estimate the maximum amount of the extracted energy for the last amplifier. The small-signal gain for a single-pass amplifier is given by [24]

$$G_0 = \exp(J_{st} l / E_s) \tag{1}$$

where J_{st} is stored energy per cm^3, l is a rod length in cm, and E_s is the saturation fluence, which for Nd:YAG is 0.66 J/cm^2 [24]. For a 6.3-mm diameter, 10-cm long rod amplifier used in the third amplifier stage, a maximum single-pass, small-signal gain of $G_0 = 6$ was achieved, which gives $J_{st} = 120$ mJ/cm^3 or 370 mJ of total stored energy in the amplifier. From Eq. (1), therefore, 10% depletion of the small-signal gain corresponds to an extracted pulse energy of 22 mJ, which is referred to here as the maximum extracted energy.

This energy can be distributed in pulses of varying temporal width as determined by the waveform driving the AOM. Figure 4 plots the temporal pulse profiles measured at the output of the AOM and at the output of the VPW laser amplifier. In this case,

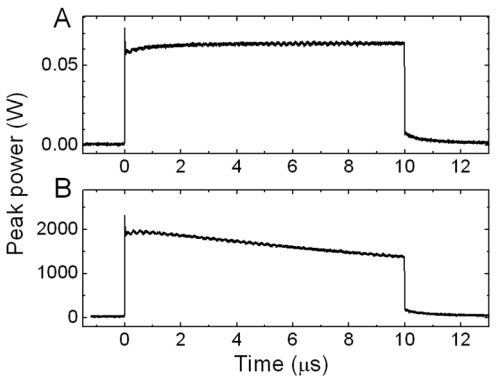

Fig. 4 Performance of VPW laser. (*a*) Output of AOM driven by rectangular pulse of 10-μs length. (*b*) Same pulses amplified through amplifier chain. Temporal profiles are measured using photodiode, and peak power is calculated from measured pulse energy.

the initial pulse out of the AOM prior to amplification is selected to be flat-top in time to test for gain depletion. The flashlamp pulse energies of the first and second amplifiers are adjusted to provide a VPW laser output pulse energy of 17 mJ for a 10-μs pulse duration, which is close to the maximum extracted energy of 22 mJ. During the first μs after amplification, the pulses have similar temporal profiles as initially generated by the AOM, and then output peak power drops by 30% toward the end of the pulse (Fig. 4(*b*)). This drop in power is larger than expected and may be attributed to the spatial profile of the beam, which is nearly Gaussian before the amplifier chain. Therefore, the central part of the Nd:YAG rod is depleted more than for the case of an ideal top-hat spatial profile. However, the ability to tailor the temporal shape of the seed pulse enables control of the final (amplified) output energy and heating rate in time. This is illustrated by the ability to generate a rising ramp function for a gradual onset of laser heating as discussed further below. Note that although the VPW laser design is similar to commercial MOPA systems (Agilite, Continuum), the commercial system requires different modulators to access a similar range of pulse durations.

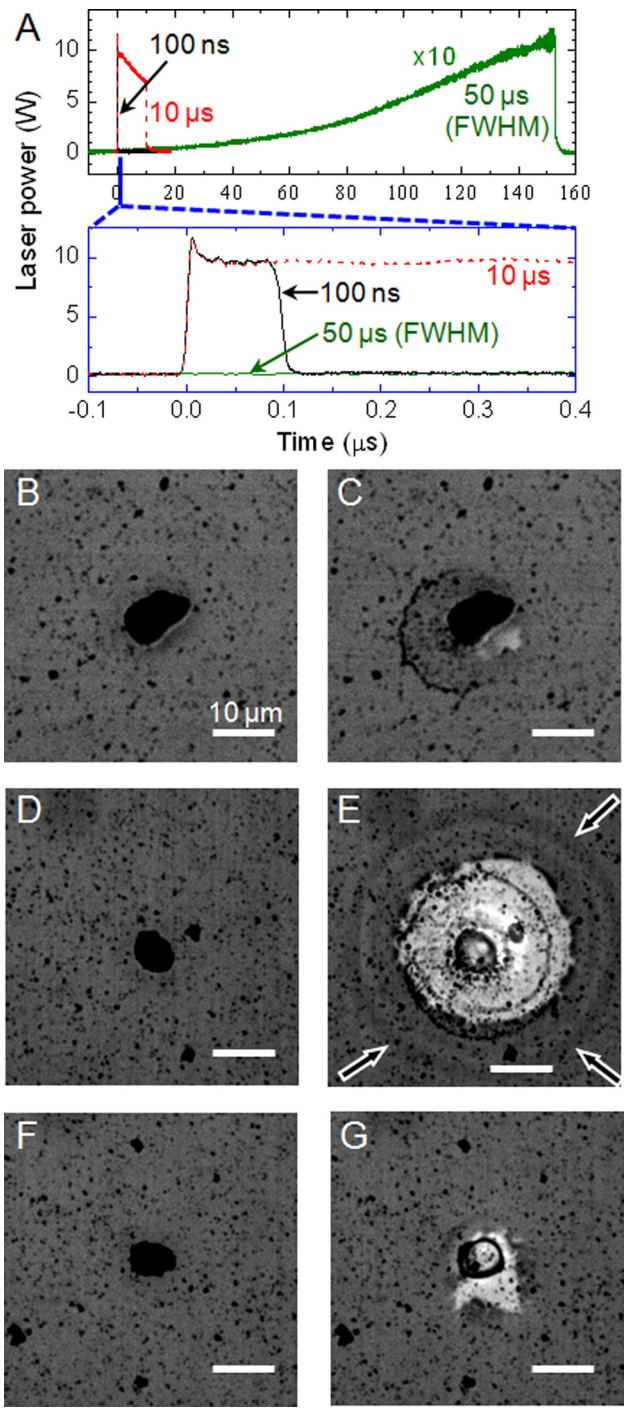

Fig. 5 Dependence of particle initiation on pulse duration and temporal profile. (*a*) Photodiode traces of 100-ns, 10-μs near-flat-top pulses, and 50-μs (FWHM) slow-rising pulse. Transmission images of aggregates before and after initiation by 100-ns, 10-μs, and 50-μs pulses are shown in (*b*) and (*c*), (*d*) and (*e*), and (*f*) and (*g*), respectively. Arrows in (*e*) point to shockwave ring. Scale bar is 10 μm.

3.2 Effect of Laser-Pulse Duration and Temporal Profile. Laser heating of aggregates consisting of 70-nm diameter Al nanoparticles was investigated by using the VPW laser to control the duration and pulse temporal profile during the initiation of aggregates. Three different pulse shapes were used to initiate 10-μm size aggregates. The first two, 100-ns and 10-μs (FWHM) pulses, had nearly flat-top temporal profiles with fast rising edges. The initial power delivered by these pulses was identical, although the total energy of the 10-μs pulse was much higher (see Fig. 5(*a*)). The third 50-μs (FWHM) long pulse was a slow-rising ramp function (150-μs total duration) with similar total energy as the 10-μs flat-top pulse. The 100-ns pulse with total energy of 0.9 μJ at the sample ablated only a small portion of the aggregate (see Figs. 5(*b*) and 5(*c*)) and resulted in a distinct ring of debris around the particle. Predictably, the 10-μs pulse with 75-μJ total energy completely disintegrated the aggregate in accordance with Fig. 1(*b*). Notably, both the 100-ns and 10-μs flat-top pulses produced a circular distribution of debris around the particle (see Figs. 5(*c*) and 5(*e*)). We attribute this effect to the initial ablation and propagation of a shockwave due to the fast (10-ns) rising edge of both pulses. The shockwave induces decomposition of the Teflon as reported previously by Yang et al. [12]. Unlike the optical images shown in Fig. 5, SEM images taken after laser initiation, as shown in Fig. 6(*a*), display an undisturbed 100-μm thick Teflon layer, indicating that these processes took place within the Teflon matrix.

The 50-μs (FWHM) pulse with a slow-rising edge and total energy of 62 μJ also shows significant destruction of the aggregate (see Figs. 5(*f*) and 5(*g*)), but with some differences compared to the results of the flat-top pulse shown in Fig. 5(*e*). Most prominent is that no shockwave ring or debris surrounding the particle is observed in the Teflon layer for the case with gradual heating (see Fig. 5(*g*)), indicative of reduced ablation. The heating rate is sufficiently slow so as to allow a significant portion of the aggregate to be heated prior to the onset of chemical reaction. Hence, much of the initiation can take place through nonablative heating. The results of this process are shown in the SEM image of Fig. 6(*b*), indicating that a significant fraction of the nanoparticle agglomerate in Fig. 5(*g*) has reacted with the Teflon matrix. The

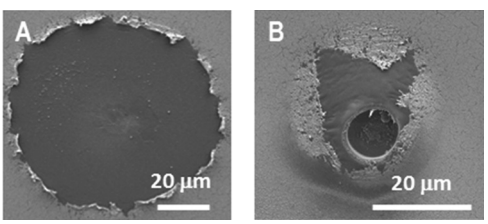

Fig. 6 SEM images of the aftermath of nanoparticle initiation for (*a*) 10-μs flat-top laser profile and (*b*) 50-μs slowly ramped pulse. The lighter outer region is the undisturbed gold coating used for enhancing contrast in the SEM images.

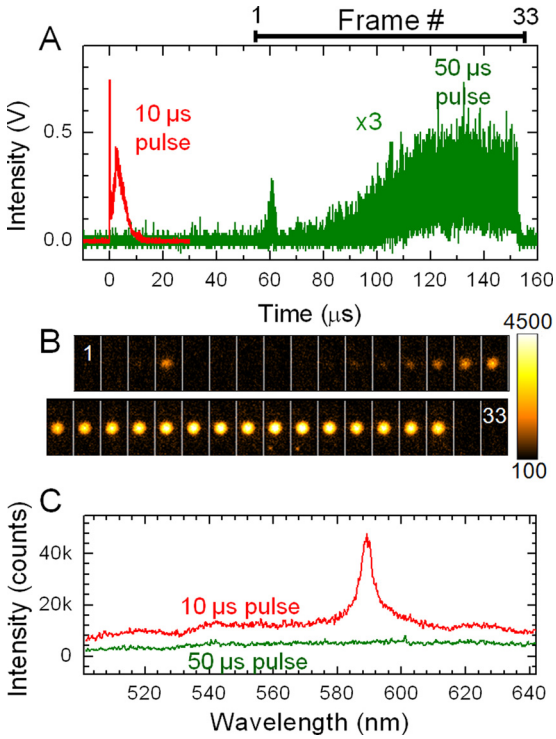

Fig. 7 Analysis of emission from laser-initiated particles. (*a*) PMT traces of emission from aggregate initiated with 10-μs flat-top laser pulse and from aggregate initiated with slow-rising 50-μs (FWHM) pulse. (*b*) 300-kHz-rate image sequence showing spatial distribution of emission from large aggregate by slow-rising 50-μs pulse. Each frame size is $15 \times 30\ \mu m^2$. Time position of images is shown in insert above PMT trace in (*a*). (*c*) Emission spectra from flat-top (10-μs) and slow-rising pulses (50-μs).

phenomena described above were consistent for nanoparticle agglomerates in the 5-μm to 15-μm size range.

To better understand differences between particle initiation by the flat-top and slow-rising pulses, we measured transient emission intensities as well as emission spectra during initiation. Figure 7(*a*) shows the time-resolved PMT measurements of the emission signal during particle initiation by the 10-μs flat-top and 50-μs slow-rising pulses. The PMT trace of the emission from the aggregate initiated with the 10-μs pulse shows a sharp, ~100-ns long initial spike in the temporal intensity trace, followed by a much broader peak in time. Similar initial spikes in integrated emission time profiles were reported in the work of Conner and Dlott [9]. The emission ceases before the end of the laser pulse likely due to complete disintegration of the aggregate during the reaction. In contrast, transient emission from the aggregate initiated by the slow-rising pulse has a delayed response with an initial burst of emission at 60 μs lasting several microseconds. This is followed by a slow-rising emission response saturating at 120 μs and an abrupt end of emission at the end of the laser pulse at 150 μs. A 300-kHz frame-rate image sequence of emission from the aggregate (Fig. 7(*b*)) closely follows the PMT trace in time.

A simultaneous spectroscopic measurement, shown in Fig. 7(*c*), displays spectrally broad emission from both the flat-top and slow-rising initiation pulses, which is in accord with previously reported data [9] and associated with hot plasma emission. However, unlike the featureless spectrum from the aggregate initiated by the slow-rising pulse, the spectrum from the aggregate initiated by the flat-top laser profile has a peak at 590 nm. This peak is assigned to Na emission that originates from the glass substrate [14,15].

Through time-gated detection of the emission (see Fig. 8), we have found that the Na peak does not occur during the initial 100-ns spike in emission after arrival of the 10-μs flat-top pulse. Rather, it occurs during the next emission peak, which is broader in time. The exact mechanism of the Na emission is unclear, but the fact that the Na emission peak is not observed for the 50-μs, slow-rising pulse confirms that its origin is associated with ablative effects upon arrival of the flat-top laser pulse. Initial damage caused by this ablation may lead to vaporization of the substrate material during the second phase of emission. These differences between laser initiation of aggregates using flat-top and slow-rising pulse profiles indicate that the nature of the initiation process is clearly dependent upon the heating rate. The ability to vary the heating rate as well as the temporal shape of the laser pulse can be used to study different regimes of laser–particle interaction, particularly for aggregates of nanoparticles. In some cases, shockwave decomposition may be of interest, while slow heating may be more appropriate for studies of nonablative heating.

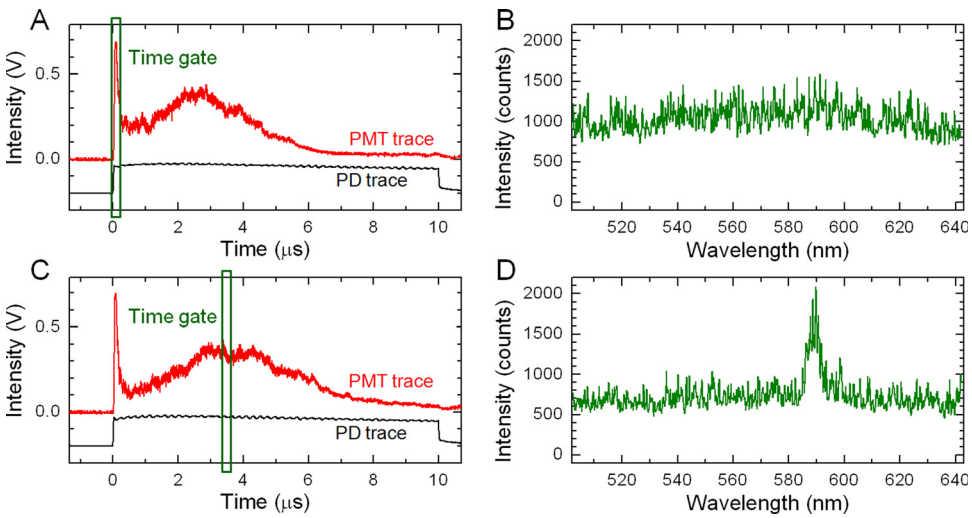

Fig. 8 Time-gated emission spectroscopy. (*a*) and (*c*) are time traces during laser–matter interaction (PMT—particle emission, PD—laser intensity). (*b*) and (*d*) are spectra collected during time gates indicated in (*a*) and (*c*), respectively. Time gates in (*a*) and (*c*) are 200 ns in duration and delayed by 0 and 3.5 μs, respectively, from the arrival of the 10-μs, 111-μJ pulse. Data are for separate realizations but show typical spectra at each time gate.

4 Conclusions

We have employed a temporally tailored variable-pulse-width laser based on a MOPA design to study the effects of heating rate on laser initiation of aggregates of Al nanoparticles. These aggregates have thermal-diffusion time scales that are much longer than the individual nanoparticles that comprise them, requiring careful consideration of the heating rate during laser initiation. Operation of the VPW laser with a micro-optical test bench allows single-particle target resolution combined with simultaneous MHz-rate imaging, time-history emission intensity measurements, and time-resolved emission spectroscopy during laser–particle interaction.

We have demonstrated that the unique ability of the VPW laser to control the temporal pulse-intensity profile and, therefore, energy-deposition rate, leads to greater control over the effects of ablative heating and the resulting shockwave propagation. The capability to control the temporal pulse shape during micro-optical initiation opens new possibilities for investigation of energetic properties for a wide range of metal nanoparticles, aggregates, and composites. This is instrumental for understanding the effects of nanoparticle composition, shape, and oxidizer matrix on laser initiation of propellant mixtures, microwelding, and laser-based nanomaterial sintering.

Acknowledgment

This work was supported, in part, by the Air Force Research Laboratory (AFRL) under Contract No. FA9300-11-M-2008 (M. Lightfoot, Technical Monitor), as well as the Air Force Office of Scientific Research (Mitat Birkan, Program Manager). J. Miller is supported by the National Science Foundation Graduate Research Fellowship program. The authors express their gratitude to W. Kulatilaka and N. Jiang of Spectral Energies, LLC; M. Lightfoot, S. Danczyk, and C. Bunker of the AFRL; W. Lewis of the University of Dayton Research Institute; S. Son of Purdue University; and V. Levitas, C. Radke, D. Diaz, B. Halls, C. Dedic, M. Cecconi, and J. Banchs-Lopez of Iowa State University for helpful discussions and technical assistance.

References

[1] Pantoya, M. L., and Granier, J. J., 2005, "Combustion Behavior of Highly Energetic Thermites: Nano Versus Micron Composites," Propellants, Explos., Pyrotech., **30**(1), pp. 53–62.

[2] Armstrong, R. W., Baschung, B., Booth, D. W., and Samirant, M., 2003, "Enhanced Propellant Combustion With Nanoparticles," Nano Lett., **3**(2), pp. 253–255.

[3] Tyagi, H., Phelan, P. E., Prasher, R., Peck, R., Lee, T., Pacheco, J. R., and Arentzen, P., 2008, "Increased Hot-Plate Ignition Probability for Nanoparticle-Laden Diesel Fuel," Nano Lett., **8**(5), pp. 1410–1416.

[4] Granier, J. J., Plantier, K. B., and Pantoya, M. L., 2004, "The Role of the Al_2O_3 Passivation Shell Surrounding Nano-Al Particles in the Combustion Synthesis of NiAl," J. Mater. Sci., **39**, pp. 6421–6431.

[5] Granier, J. J., and Pantoya, M. L., 2004, "Laser Ignition of Nanocomposite Thermites," Combust. Flame, **138**(4), pp. 373–383.

[6] Granier, J. J., Mullen, T., and Pantoya, M. L., 2003, "Nonuniform Laser Ignition in Energetic Materials," Combust. Sci. Technol., **175**(11), pp. 1929–1951.

[7] Surber, E., Lozano, A., Lagutchev, A., Kim, H., and Dlott, D. D., 2007, "Surface Nonlinear Vibrational Spectroscopy of Energetic Materials: HMX," J. Phys. Chem. C, **111**(5), pp. 2235–2241.

[8] Sanders, V. E., Asay, B. W., Foley, T. J., Tappan, B. C., Pacheco, A. N., and Son, S. F., 2007, "Reaction Propagation of Four Nanoscale Energetic Composites (Al/MoO_3, Al/WO_3, Al/CuO, and Bi_2O_3)," J. Propul. Power, **23**, pp. 707–714.

[9] Conner, R. W., and Dlott, D. D., 2010, "Ultrafast Condensed-Phase Emission From Energetic Composites of Teflon and Nanoaluminum," J. Phys. Chem. A, **114**(25), pp. 6731–6741.

[10] Zamkov, M. A., Conner, R. W., and Dlott, D. D., 2007, "Ultrafast Chemistry of Nanoenergetic Materials Studied by Time-Resolved Infrared Spectroscopy: Aluminum Nanoparticles in Teflon," J. Phys. Chem. C, **111**(28), pp. 10278–10284.

[11] Dlott, D. D., 2006, "Thinking Big (and Small) About Energetic Materials," Mater. Sci. Technol., **22**, pp. 463–473.

[12] Yang, Y., Wang, S., Sun, Z., and Dlott, D. D., 2004, "Propagation of Shock-Induced Chemistry in Nanoenergetic Materials: The First Micrometer," J. Appl. Phys., **95**(7), pp. 3667–3676.

[13] Moore, D. S., Son, S. F., and Asay, B. W., 2004, "Time-Resolved Spectral Emission of Deflagrating Nano-Al and Nano-MoO_3 Metastable Interstitial Composites," Propellants, Explos. Pyrotech., **29**(2), pp. 106–111.

[14] Yang, Y., Sun, Z., Wang, S., and Dlott, D. D., 2003, "Fast Spectroscopy of Laser-Initiated Nanoenergetic Materials," J. Phys. Chem. B, **107**(19), pp. 4485–4493.

[15] Wang, S., Yang, Y., Sun, Z., and Dlott, D. D., 2003, "Fast Spectroscopy of Energy Release in Nanometric Explosives," Chem. Phys. Lett., **368**(1-2), pp. 189–194.

[16] Wang, S., Yang, Y., Yu, H., and Dlott, D. D., 2005, "Dynamical Effects of the Oxide Layer in Aluminum Nanoenergetic Materials," Propellants, Explos. Pyrotech., **30**(2), pp. 148–155.

[17] Efimov, O., Juodkazis, S., and Misawa, H., 2004, "Intrinsic Single- and Multiple-Pulse Laser-Induced Damage in Silicate Glasses in the Femtosecond-to-Nanosecond Region," Phys. Rev. A, **69**(4), p. 042903.

[18] Stuart, B. C., Feit, M. D., Rubenchik, A. M., Shore, B. W., and Perry, M. D., 1995, "Laser-Induced Damage in Dielectrics With Nanosecond to Subpicosecond Pulses," Phys. Rev. Lett., **74**(12), pp. 2248–2251.

[19] Salimbeni, R., Pini, R., and Siano, S., 2003, "A Variable Pulse Width Nd:Yag Laser for Conservation," J. Cultural Heritage, **4**(Supplement 1), pp. 72–76.

[20] Garnov, S. V., Konov, V. I., Kononenko, T., Pashinin, V. P., and Sinyavsky, M. N., 2004, "Microsecond Laser Material Processing at 1.06 μm," Laser Phys., **14**(6), pp. 910–915.

[21] Miller, J. D., Slipchenko, M. N., Meyer, T. R., Jiang, N., Lempert, W. R., and Gord, J. R., 2009, "Ultrahigh-Frame-Rate OH Fluorescence Imaging in Turbulent Flames Using a Burst-Mode Optical Parametric Oscillator," Opt. Lett., **34**(9), pp. 1309–1311.

[22] Yang, Y., Wang, S., Sun, Z., and Dlott, D. D., 2004, "Near-Infrared Laser Ablation of Poly Tetrafluoroethylene (Teflon) Sensitized by Nanoenergetic Materials," Appl. Phys. Lett., **85**(9), pp. 1493–1495.

[23] Dreizin, E. L., 2009, "Metal-Based Reactive Nanomaterials," Prog. Energy Combust. Sci., **35**(2), pp. 141–167.

[24] Koechner, W., 2006, *Solid-State Laser Engineering* (Optical Sciences), Springer, New York.